Single-Nanoparticle Detection Using a Low-Aspect-Ratio Pore

Makusu Tsutsui,[†] Sadato Hongo,[‡] Yuhui He,[†] Masateru Taniguchi,[†,*] Nobuhiro Gemma,[‡] and Tomoji Kawai[†,*]

[†]The Institute of Scientific and Industrial Research, Osaka University, Ibaraki, Osaka 567-0047, Japan and [‡]Corporate Research & Development Center, Toshiba Corporation, Kawasaki, Kanagawa 212-8582, Japan

ABSTRACT

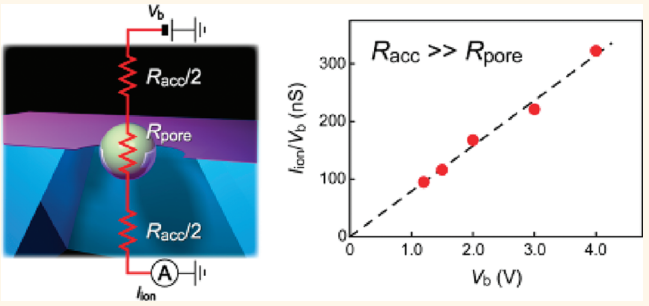

We explored single-particle translocation through a low thickness-to-diameter aspect ratio Si_3N_4 pore mimicking graphene nanopore structure by a resistive pulse method. Ionic conductance of 0.05 aspect ratio pores scales linearly with the diameter, indicating predominant contribution of the access resistance to the ion transport. We find that the access resistance changes little during particle translocation. Furthermore, we observe enhanced particle capture rates *via* the strong electric field extended outside the low-aspect-ratio pore mouth. We also demonstrate electrical discrimination of two different sized particles using the low-aspect-ratio pore sensor with the constant access resistance assumption. The present findings indicate the potential utility of nucleotide-sized graphene nanopores as an electrical sensing platform for single-base identification *via* transmembrane ionic current blockade detections.

KEYWORDS: solid-state nanopore · access resistance · low aspect ratio · ionic current blockage · single-particle detection

A single pore formed in an insulating membrane has been exploited as a useful system for studying physics underlying the electric field-driven translocation of an individual molecule or particle at the nanoscale.[1−5] The single-particle sensing mechanism involves detection of temporal change in the transmembrane ion transport associated with the volume exclusion effects of a molecule passing through the pore.[1−5] A promising application of the pore sensor is electrical DNA sequencing.[6−14] It has recently been demonstrated that a partial blockage of the ion current through a biologically engineered α-hemolysin channel during single nucleotide translocation enables direct identification of the four base molecules.[7,15] However, nanopore sequencing is yet to be achieved because of the fact that DNA molecules thread through the biological pores too fast to interrogate the base sequence for the limited bandwidth (<10 MHz) of current measurement systems.[2,5,16] This has led to growing interest in pursuing the development of solid-state nanopore sensors with high spatial sensitivity, as they are more mechanically robust and configurable to incorporate molecular translocation speed controllability.[16−21]

The spatial resolution of a nanopore device is determined by the thickness of the membrane. From this respect, graphene is considered as a potential material for attaining single-base resolution, because of the excellent mechanical strength and the well-defined single-atom sheet structure ideal for attaining single-base resolution.[5] To date, fabrication of a nanoscale pore in a single-layered or multilayered graphene membrane has been realized by several research groups using an electron beam sculpting technique.[22−26] Though not yet sequencing, the atomically thin nanopores were also found to be applicable for single-molecule detection of double-stranded DNA.[23−25]

Despite that graphene nanopores offer prospective direct sequencing *via* the ionic current blockage,[25] particle capture/translocation kinetics and its influence on the ion transport in such an unusually low aspect ratio pore have not been addressed. It is anticipated that the resistivity of the electrolyte solution outside the pore, the so-called access resistance,[27] becomes non-negligible when seeking to achieve high spatial resolution by shrinking the membrane thickness, as it leads to decreased cross-pore resistance. Here, we investigated single-particle translocation in a low-aspect-ratio solid-state pore mimicking the graphene

* Address correspondence to taniguti@sanken.osaka-u.ac.jp.

Received for review February 5, 2012 and accepted March 17, 2012.

Published online March 18, 2012
10.1021/nn300530b

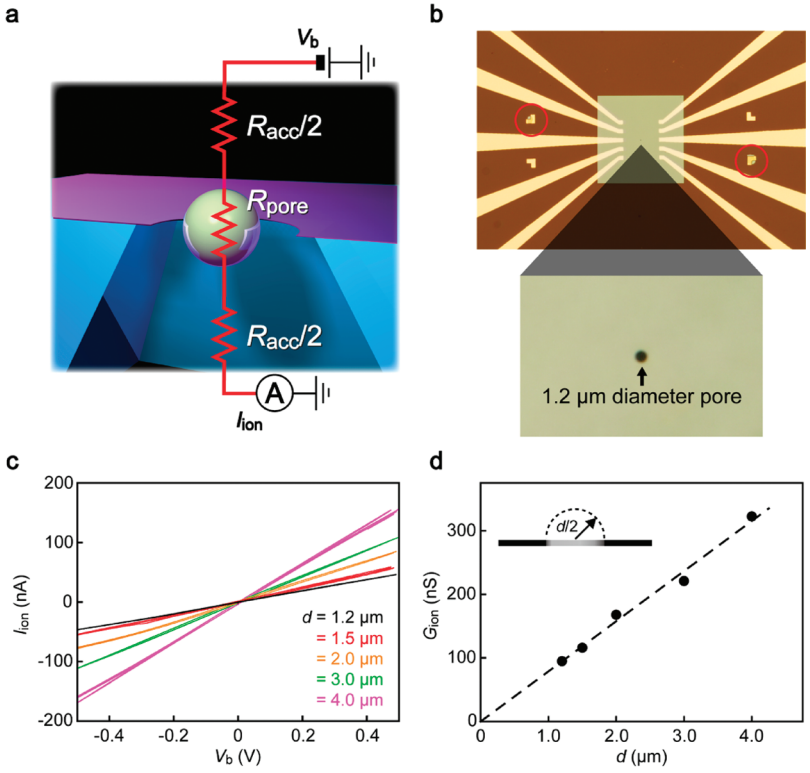

Figure 1. Structure and open pore conductance of low-aspect-ratio pores. (a) Schematic description of thin Si_3N_4 micropore. The transmembrane ionic resistance is defined by the cross-pore resistance, R_{pore}, and the access resistance, R_{acc}, connected in series. In experiments, the transmembrane current, I_{ion}, is measured under a dc voltage V_b. (b) Optical microscope image of a 1.2 μm diameter pore formed in a 50 nm thick Si_3N_4 membrane. The L-shaped external markers at both sides were utilized as a guide to delineate the micropore at the center of the membrane by electron beam lithography. (c) $I_{ion}-V_b$ characteristics of the low-aspect-ratio pores acquired in a TE buffer. (d) Plots of the pore conductance, G_{ion}, obtained from the slope of the $I_{ion}-V_b$ curves in (c), as a function of the pore diameter, d. Dashed line is a linear fit. The linear $G_{ion}-d$ dependence manifests a predominant role of R_{acc}. Inset depicts the hemisphere extending outside a low-aspect-ratio pore indicated by a dotted curve. The ion conductivity inside and outside the hemisphere defines $R_{acc} = \rho/d$, where ρ is the resistivity of the ionic solution.

nanopore architecture wherein the access resistance, R_{acc}, rather than the pore resistance, R_{pore}, dominates the open pore ion transport (Figure 1a).

RESULTS AND DISCUSSION

The micropore sensors were first calibrated by measuring $I_{ion}-V_b$ characteristics in a TE buffer (10 mM Tris-hydrochloride, 1 mM EDTA, pH 8.0). We obtained a linear increase in I_{ion} with V_b for pores with d = 6.0 to 1.2 μm (Figure 1c). Plots of the pore conductance G estimated from linear fits to the $I_{ion}-V_b$ curves against d reveal linear $G-d$ dependence (Figure 1d). The whole resistance $R = 1/G$ between the two electrophoretic electrodes can be described as $R = R_{acc} + R_{pore}$. The cross-pore resistance R_{pore} for the micropore immersed in an electrolyte solution with the resistivity ρ is written as $R_{pore} = 4\rho L/\pi d^2$, where L = 50 nm is the thickness of the pore. On the other hand, R_{acc} is defined as $R_{acc} = \rho/d$. Therefore, the linear $G-d$ relation manifests the predominant role of the ionic resistance outside the pore on I_{ion},[27] a unique behavior observed also in graphene nanopores.[25] The slope of the $G-d$ plots gives ρ = 12.7 Ωm, which is typical for the resistivity of TE buffer (10–20 Ωm).

We utilized the low-aspect-ratio pore of size d = 1.2 μm and L = 50 nm for detection of 0.78 μm sized polystyrene (Pst) particles in a solution at a concentration of 0.3 pM. We observed current spikes signifying temporal ionic current blockage by volume exclusion effects of the polymer beads in the pore in a V_b range from 0.05 to 0.27 V (Figure 2a).[29] The current blockade signals can be characterized by the spike height I_p and width t_d (Figure 2b). The I_p distributions show a single-peak structure. The peak current I_{Pst} was extracted from the I_p distributions acquired at various V_b conditions by Gaussian fitting (Figure 2c). We find a linear $I_{Pst}-V_b$ relation at the low-V_b regime below 0.23 V (Figure 2d, red plots). These plots are in good agreement with a theoretical estimation of $R_{acc} = \rho/d$ = 9.5 MΩ and $R_{pore} = 4\rho L/\pi d^2$ = 0.49 MΩ (0.81 MΩ) in the 1.24 μm pore without (with) a 0.78 μm Pst particle in a solution of ρ = 11.8 Ωm (dashed line in Figure 2d). The open pore current, I_0, is also reproduced using the same ρ and d (Figure 2d inset). This in turn indicates that R_{acc} of the low-aspect-ratio micropore remains unaltered during particle translocation.

We further examined the role of R_{acc} on a single-particle detection *via* the ion blockade mechanism by

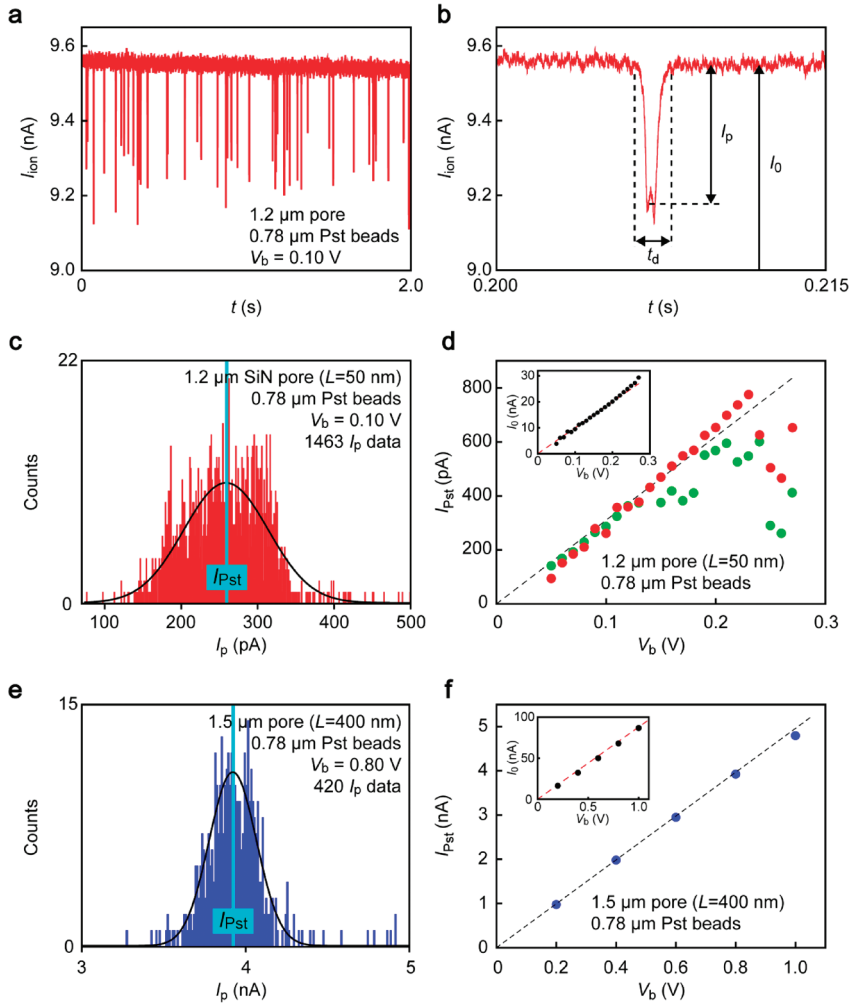

Figure 2. Single-particle detection using the low-aspect-ratio pore sensors. (a) I_{ion}−t curve measured using the low-aspect-ratio pore of diameter d = 1.2 μm and thickness L = 50 nm in a TE buffer solution containing 0.78 μm sized polystyrene (Pst) beads at a concentration of 0.3 pM under an electrophoretic voltage V_b = 0.1 V. Current spikes were observed signifying single-particle translocation. (b) Magnified view of I_{ion} spike that is characterized by the width t_d and height I_p from the base level current I_0 representing the trapping duration and the ion exclusion effect by the particle in the pore, respectively. (c) Distribution of I_p data extracted from the I_{ion}−t trace for 0.78 μm Psts at V_b = 0.10 V. Peak current I_{Pst} was obtained by Gaussian fitting to the histogram (black curve). (d) I_{Pst} *versus* V_b plots at two different particle solution concentration conditions, 0.3 pM (red) and 0.03 pM (green), showing a linear increase in the blockade current with the applied voltage at V_b < 0.23 V. Black dashed line is obtained by the series resistance model calculation using ρ = 11.8 Ωm and d = 1.24 μm. Inset is the background current I_0 plotted with respect to V_b. The red dashed line is a linear fit. (e) I_p histograms constructed with current spikes measured in 0.78 μm Psts using a high-aspect-ratio pore of d = 1.5 μm and L = 400 nm and (f) corresponding I_{Pst}−V_b plots. Black dashed line is drawn based on the series resistance model calculation with ρ = 14.0 Ωm and d = 1.68 μm. Inset is the I_0−V_b plots. Red dashed line is a linear fit.

exhibiting the I_p measurements with a higher aspect ratio micropore sensor (d = 1.5 μm and L = 400 nm). I_{ion}−t traces obtained in a 0.78 μm Pst solution (concentration is 10^9 particle/mL) show current spikes. The corresponding I_p histograms at V_b = 0.2 to 1.0 V reveal a single-peak profile (Figure 2e). We plotted I_{Pst} as a function of V_b (Figure 2f). Similar to the case for the low-aspect-ratio pore, the linear I_{Pst}−V_b dependence complies with the series resistance model that yields R_{acc} = 8.3 MΩ and R_{pore} = 2.5 MΩ (3.1 MΩ) using ρ = 14.0 Ωm and d = 1.68 μm without (with) a 0.78 μm polymer particle. The fact that the estimated diameter is larger than the nominal value is ascribable to over-etching during the reactive ion etching process used for drilling the pore. The open pore current also agrees with the R_{acc} and R_{pore} as displayed in the inset of Figure 2f. These results serve to corroborate the constant nature of the access resistance during single-particle translocation.

In addition to the signal interpretation, the particle capture efficiency is a practically important issue for high-throughput nanopore sensors.[30,31] The average signal frequency, or equivalently the particle capture rate, was found to be f_{cap} = 14 signals/s and 2 signals/s at V_b = 0.05 V for the I_{ion}−t curves acquired using the low-aspect-ratio 1.2 μm pores in a TF buffer solution containing 0.78 μm Pst beads at the concentration N of 0.3 and 0.03 pM, respectively. This suggests a linear

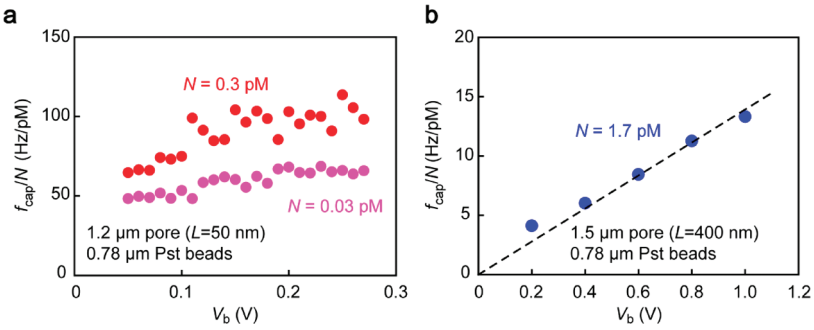

Figure 3. Role of the access resistance on particle capture kinetics. (a) Specific capture rate f_{cap}/N for 0.78 μm Psts in the low-aspect-ratio pore (d = 1.2 μm and L = 50 nm) plotted against V_b. (b) $f_{cap}/N-V_b$ characteristics for 0.78 μm Psts in the high-aspect-ratio pore (d = 1.5 μm and L = 400 nm). Black dashed line is a linear fit.

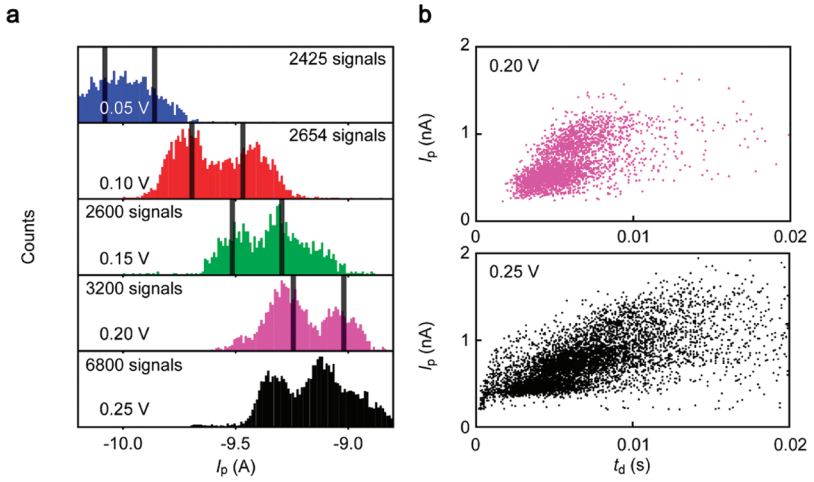

Figure 4. Single-particle size discrimination by blockade current measurements. (a) Blockade current histograms constructed with I_p data obtained at 0.05 V $\leq V_b \leq$ 0.25 V in a TE solution mixture containing equimolar 0.78 and 0.90 μm Pst beads at a net concentration of 0.3 pM using the low-aspect-ratio pore (d = 1.2 μm and L = 50 nm). The bimodal distributions reflect translocation of different sized particles through the pore. Black bands are the blockade current deduced by the series resistance model calculations for the two particles under a fixed pore diameter d = 1.2 μm and with ρ ranging from 12 to 20 Ωm. The relative peak positions are in good agreement with the theoretical estimation. (b) I_p-V_b scatter plots at V_b = 0.20 V (top) and 0.25 V (bottom).

relation between f_{cap} and the bulk particle concentration.[32] We also find that the specific capture rate f_{cap}/N increases with the electrophoretic voltage in the V_b range measured. It has been established that the capture rate scales in two different manners with the electric field along a pore depending on whether the electrophoretic force is strong enough to overcome the energy barrier E_B at the mouth against particle capture or not.[33] Under low-V_b conditions, the effective barrier height is diminished with the applied voltage, leading to a sharp increase in the rate of capture with V_b. On the other hand, in a high-V_b regime wherein the electrophoretic voltage more than compensates the barrier energy, the capture efficiency increases little with V_b since the probability of particle translocation once it enters the pore is already close to unity. In Figure 3a, f_{cap}/N increases only gradually with V_b, which implies the saturation regime of the translocation probability where $eV_b > E_B$. On the other hand, f_{cap}/N in a high-aspect-ratio 1.5 μm pore at N = 1.7 pM shows linear dependence on V_b from f_{cap} = 0 Hz, suggesting that $eV_b < E_B$, wherein the electric-field-driven barrier energy crossover processes dominate the single-particle capture kinetics.[30,33] The essential difference between the two types of pores may lie in the fact that the electric field extending outside the pore is stronger for the 50 nm thick pores with larger R_{acc}-to-R_{pore} ratio, which facilitates the particle translocation.[31]

The low-aspect-ratio pore was used for discrimination of Pst particles of different sizes. We measured I_{ion} in a TE solution containing an equal amount of 0.78 and 0.90 μm Pst beads. Bimodal I_p histograms were obtained. The peak positions of these I_p distributions at $V_b \leq$ 0.20 V were in good accordance with R_{acc} and R_{pore} deduced by the series resistance model for the two different polymer particles (black bars in Figure 4a).

While we have seen so far that current blockade events in the linear $I_{Pst}-V_b$ regime can be interpreted by the series resistance model with a constant access resistance assumption, a peculiar feature always

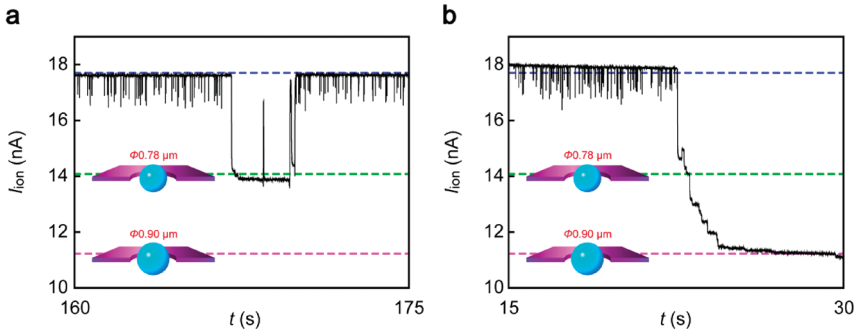

Figure 5. Pore-blocking events. (a) Temporal stacking and (b) complete pore-blocking events observed during I_{ion} measurements using a 1.0 μm pore in a TE solution mixture of 0.78 and 0.90 μm Pst beads. Green and purple dashed lines denote the ion current level estimated by the multiphysics model calculation for a $d = 1.2$ μm and $L = 50$ nm micropore system with 0.78 and 0.90 μm spherical particles placed at the center, respectively. Blue dashed line is the open pore current estimated with the same model but without a particle.

appeared at the high-field conditions; I_{Pst} suddenly starts to decrease at $V_b > 0.23$ V. The unexpected high-field characteristic is reproduced even in the I_p measurements conducted in the solution mixture of two different sized particles (Figure 4a). It is noticeable that I_0 scales linearly with V_b in the voltage range measured (Figure 2d inset), in accordance with the $I_{ion}-V_b$ characteristics in Figure 2c. Therefore, the high-bias anomaly cannot be attributed to a field-induced change in the ion mobility in the low-aspect-ratio pore at $V_b >$ 0.23 V. Rather, it is more likely to be attributed to translocation processes of the polymer particles. Scatter plots of I_p *versus* t_d in Figure 4b already reveal a change in the particle translocation processes at $V_b >$ 0.2 V; although 0.78 μm and 0.90 μm particles can be discerned by the two event clusters observed in the diagrams at $V_b = 0.20$ and 0.25 V, the data are conspicuously scattered more extensively at $V_b = 0.25$ V. Especially, there is an increasing number of short events with relatively small current blockages. These data would correspond to translocation blocking events by random collisions at the vicinity of the pore among several particles electrically attracted to the pore at the same time. Conversely, the long events with high I_p may originate from simultaneous crossing of several particles. Eventually, the overall distribution of I_p fluctuates at the high-bias regime, as we have seen in Figure 2d. The fact that I_{Pst} decreases at the high biases suggests a predominant influence of the many-body collision effects. The absence of the high-bias feature in the high-aspect-ratio pores can be understood by the inadequate electrophoretic driving force for letting multiple particles surpass the energy barrier and be captured together in the pore within a short range of time.[31,33]

Despite that the constant R_{acc} model explains most of the experimental results, such an ideal situation is counterintuitive, as it is expected *a priori* that the access resistance increases to some extent when a particle partially occupies the hemispheres at the pore entrance possessing about half of the total access resistance[27] and excludes the ions there (in a similar manner to that of the ion exclusion effects on R_{pore}). In fact, our multiphysics model calculations of the blockade current based on self-consistent ion transport derivation[31] using Navier–Stokes, Nernst–Plank, and Poisson equations derive a higher I_p than what we obtained from the series resistance model: The multiphysics model calculations give $I_p = 2.33$ nA, whereas the series resistance model with a constant R_{acc} assumption estimates $I_p = 0.64$ nA for a 0.78 μm particle translocation through a $d = 1.2$ μm and $L = 50$ nm pore, while both models give a similar background current of $I_0 \approx 20$ nA. This predicts that the access resistance should change appreciably at least under a static point of view wherein ion transport takes place through the pore with a particle located at the center. Interestingly, we find an I_p that matches well with the multiphysics model estimation for temporal stacking or complete blocking events detected during 0.78 and 0.90 μm polymer bead translocation through a 1.0 μm pore (Figure 5a,b). Particle stacking was confirmed by reversing the direction of the electrophoretic field after the permanent decrease in I_{ion}, which led to removal of the trapped particle and concomitant recovery of the original background current level. We speculate that the access resistance responds dynamically to the ion exclusion in the hemisphere by the particles upon translocation and gives rise to fluctuations of I_{ion}, but the effect on I_p is moderate unless they are swiftly moving without being stacked in the pore due presumably to a relaxation of ion distributions or contributions of counterions on the particle surface.

CONCLUSION

In summary, we have studied the single-particle translocation through low-aspect-ratio pores. The pore conductance in a low thickness-to-diameter aspect ratio ranges less than 0.05 scaled linearly with the pore diameter, suggesting an access resistance dominant regime of the ion transport. The low-aspect-ratio pore sensor can be used to identify polymer beads of

different sizes by measuring the blockade current associated with ion exclusion by particles in the pores. In these experiments, the access resistance was found to remain constant during particle translocation as long as they are not trapped in the pore. The invariance of access resistance is a favorable condition for single-molecule detection by the resistive pulse technique using low-aspect-ratio nanopore sensors and opens the prospect of graphene nanopore sequencing though the influence of the untranslocated portion of DNA outside the pore on the translocation dynamics and the pore resistance.[34,35]

METHODS

Fabrication of Low-Aspect-Ratio Pores. We fabricated a micropore in a thin Si_3N_4 membrane with a thickness-to-diameter aspect ratio less than 0.1 as follows. A 0.8 mm square region of the unpolished side of a Si_3N_4 (50 nm)/Si (0.5 mm)/Si_3N_4 (50 nm) wafer was exposed to reactive ion etching (CF_4, 100 W) to partially remove the Si_3N_4 layer. We then wet-etched the exposed 0.5 mm thick Si layer by a KOH solution at 90 °C. As a result, we obtained a 50 nm thick, 100 μm $\times$ 100 μm Si_3N_4 membrane (Figure 1b). After that, we patterned a circle of diameter d = 1.0 to 6.0 μm in a resist layer (ZEP520A) coated on the substrate using an electron beam lithography process. Subsequently, a micropore of diameter d was sculpted by exposing the substrate to reactive ion etching (CF_4, 100 W). Finally, the residual resist layer was removed by immersing the sample in *N*,*N*-dimethylformamide for 8 h followed by oxygen plasma cleaning. This yields Si_3N_4 micropores with an aspect ratio less than 0.05, which corresponds to a 6 nm sized graphene nanopore.

Pore Device Sealing and Single-Particle Detections. In our experiments, we adhered polydimethylsiloxane (PDMS) blocks onto which a microchannel was patterned at both sides of the pore device. Specifically, we prepared an SU-8 mold on a Si/SiO_2 wafer using a photolithography method. PDMS (Sylgard 184) was cured on the mold at 70 °C for 1 h. Three holes were pierced in each PDMS block: one for placing a Ag/AgCl electrode and two for the inlet and outlet of particle solution. The PDMS channel and the sample substrate were treated with oxygen plasma for surface activation[28] and attached together to obtain permanent bonding between PDMS and Si_3N_4. Carboxyl-functionalized polystyrene microbeads of size 0.78 and 0.90 μm were employed as target particles. These particles were dispersed in a TE buffer (10 mM Tris-HCl, 1 mM EDTA, pH 8.0). We introduced the particle-dispersed solution in the *trans* chamber and buffer solution in the *cis* chamber *via* the PDMS channel. For single-particle detection, the electrophoretic field V_b was applied to the pore utilizing two Ag/AgCl electrodes at both sides, and the transmembrane ionic current, I_{ion}, was monitored at 1 MHz employing a home-built current amplifier backed by a digitizer (National Instruments NI-5922) and stored in a RAID hard drive (National Instruments HDD-8265) under LabVIEW control.

Conflict of Interest: The authors declare no competing financial interest.

Acknowledgment. This research is partially supported by the Japan Society for the Promotion of Science (JSPS) through its Funding Program for World-Leading Innovative R&D on Science and Technology.

REFERENCES AND NOTES

1. Dekker, C. Solid State Nanopores. *Nat. Nanotechnol.* **2007**, *2*, 209.
2. Branton, D.; Deamer, D. W.; Marziali, A.; Bayley, H.; Benner, S. A.; Butler, T.; Di Ventra, M.; Garaj, S.; Hibbs, A.; Huang, X.; et al. The Potential and Challenges of Nanopore Sequencing. *Nat. Biotechnol.* **2008**, *26*, 1146.
3. Zwolak, M.; Di Ventra, M. Colloquium: Physical Approaches to DNA Sequencing and Detection. *Rev. Mod. Phys.* **2008**, *80*, 141.
4. Deamer, D. NanoporeAnalysis of Nucleic Acids Bound to Exonucleases and Polymerases. *Annu. Rev. Biophys.* **2010**, *39*, 79–109.
5. Venkatesan, B. M.; Bashir, R. Nanopore Sensors for Nucleic Acid Analysis. *Nat. Nanotechnol.* **2011**, *6*, 615–624.
6. Kasianowicz, J. J.; Brandin, E.; Branton, D.; Deamer, D. W. Characterization of Individual Polynucleotide Molecules Using a Membrane Channel. *Proc. Natl. Acad. Sci.* **1996**, *93*, 13770–13773.
7. Clarke, J.; Wu, H.-C.; Jayasinghe, L.; Patel, A.; Reid, S.; Bayley, H. Continuous Base Identification for Single-Molecule Nanopore DNA Sequencing. *Nat. Nanotechnol.* **2009**, *4*, 265–270.
8. Derrington, I. M.; Butler, T. Z.; Collins, M. D.; Manrao, E.; Pavlenok, M.; Niederweis, M.; Gundlach, J. H. Nanopore DNA Sequencing with MspA. *Proc. Natl. Acad. Sci.* **2010**, *107*, 16060–16065.
9. Lieberman, K. R.; Cherf, G. M.; Doody, M. J.; Olasagasti, F.; Kolodji, Y.; Akeson, M. Processive Replication of Single DNA Molecules in a Nanopore Catalyzed by Phi29 DNA Polymerase. *J. Am. Chem. Soc.* **2010**, *132*, 17961–17972.
10. Postma, H. W. Ch. Rapid Sequencing of Individual DNA Molecules in Graphene Nanogaps. *Nano Lett.* **2010**, *10*, 420–425.
11. Tsutsui, M.; Taniguchi, M.; Yokota, K.; Kawai, T. Identifying Single Nucleotides by Tunnelling Current. *Nat. Nanotechnol.* **2010**, *5*, 286–290.
12. Huang, S; He, J.; Chang, S.; Zhang, P.; Liang, F.; Li, S.; Tuchband, M.; Fuhrmann, A.; Ros, R.; Lindsay, S. Identifying Single Bases in a DNA Oligomer with Electron Tunnelling. *Nat. Nanotechnol.* **2010**, *5*, 868–873.
13. Ivanov, A. P.; Instuli, E.; McGilvery, C.; Baldwin, G.; McComb, D. W.; Albrecht, T.; Edel, J. B. DNA Tunneling Detector Embedded in a Nanopore. *Nano Lett.* **2011**, *11*, 279–285.
14. Xie, P.; Xiong, Q.; Fang, Y.; Qing, Q.; Lieber, C. M. Local Electrical Potential Detection of DNA by Nanowire-Nanopore Sensors. *Nat. Nanotechnol.* **2012**, *7*, 119–125.
15. Stoddart, D.; Heron, A. J.; Mikhailova, E.; Maglia, G.; Bayley, H. Single-Nucleotide Discrimination in Immobilized DNA Oligonucleotides with a Biological Nanopore. *Proc. Natl. Acad. Sci. U. S. A.* **2009**, *106*, 7702–7707.
16. Keyser, U. F. Controlling Molecular Transport through Nanopores. *J. R. Soc. Interface* **2011**, *8*, 1369–1378.
17. Keyser, U. F.; Koeleman, B. N.; van Dorp, S.; Krapf, D.; Smeets, R. M. M.; Lemay, S. G.; Dekker, N. H.; Dekker, C. Direct Force Measurements on DNA in a Solid-State Nanopore. *Nat. Phys.* **2006**, *2*, 473–477.
18. Fologea, D.; Uplinger, J.; Thomas, B.; McNabb, D. S.; Li, J. Slowing DNA Translocation in a Solid-State Nanopore. *Nano Lett.* **2005**, *5*, 1734–1737.
19. Iqbal, S. M.; Akin, D.; Bashir, R. Controlling Protein Translocation through Nanopores with Bio-Inspired Fluid Walls. *Nat. Nanotechnol.* **2011**, *6*, 253–260.
20. Luan, B.; Peng, H.; Polonsky, S.; Rossnagel, S.; Stolovitzky, G.; Martyna, G. Base-by-Base Ratcheting of Single Stranded DNA through a Solid-State Nanopore. *Phys. Rev. Lett.* **2010**, *104*, 238103.
21. He, Y.; Tsutsui, M.; Fan, C.; Taniguchi, M.; Kawai, T. Controlling DNA Translocation through Gate Modulation of Nanopore Wall Surface Charges. *ACS Nano* **2011**, *5*, 5509–5518.
22. Fischbein, M. D.; Drndic, M. Electron Beam Nanosculpting of Suspended Graphene Sheets. *Appl. Phys. Lett.* **2008**, *93*, 113107–113103.

23. Merchant, C. A.; Healy, K.; Wanunu, M.; Ray, V.; Peterman, N.; Bartel, J.; Fischbein, M. D.; Venta, K.; Luo, Z.; Johnson, A. T. C.; *et al*. DNA Translocation through Graphene Nanopores. *Nano Lett.* **2010**, *10*, 2915.
24. Schneider, G. F.; Kowalczyk, S. W.; Calado, V. E.; Pandraud, G.; Zandbergen, H. W.; Vandersypen, L. M. K.; Dekker, C. DNA Translocation through Graphene Nanopores. *Nano Lett.* **2010**, *10*, 3163.
25. Garaj, S.; Hubbard, W.; Reina, A.; Kong, J.; Branton, D.; Golovchenko, J. A. Graphene as a Subnanometre Trans-Electrode Membrane. *Nature* **2010**, *467*, 190.
26. Song, B.; Schneider, G. F.; Xu, Q.; Pandraud, G.; Dekker, C.; Zandbergen, H. Atomic-Scale Electron-Beam Sculpting of Near-Defect-Free Graphene Nanostructures. *Nano Lett.* **2011**, *11*, 2247–2250.
27. Hall, J. E. Access Resistance of a Small Circular Pore. *J. Gen. Physiol.* **1975**, *66*, 531–532.
28. Bhattacharya, S.; Datta, A.; Berg, J. M.; Gangopadhyay, S. Studies on Surface Wettability of Poly(dimethyl) Siloxane (PDMS) and Glass under Oxygen-Plasma Treatment and Correlation with Bond Strength. *J. Microelectron. Syst.* **2005**, *14*, 590–597.
29. Lan, W.-J.; Holden, D. A.; Zhang, B.; White, H. S. Nanoparticle Transport in Conical-Shaped Nanopores. *Anal. Chem.* **2011**, *83*, 3840–3847.
30. Wanunu, M.; Morrison, W.; Rabin, Y.; Grosberg, A. Y.; Meller, A. Electrostatic Focusing of Unlabelled DNA into Nanoscale Pores using a Salt Gradient. *Nat. Nanotechnol.* **2009**, *5*, 160–165.
31. He, Y.; Tsutsui, M.; Fan, C.; Taniguchi, M.; Kawai, T. Gate Manipulation of DNA Capture into Nanopores. *ACS Nano* **2011**, *5*, 8391–8397.
32. Wanunu, M.; Dadosh, T.; Ray, V.; Jin, J.; McReynolds, L.; Drndic, M. Rapid Electronic Detection of Probe-Specific MicroRNA using Thin Nanopore Sensors. *Nat. Nanotechnol.* **2010**, *5*, 807–814.
33. Matysiak, S.; Montesi, A.; Pasquali, M.; Kolomeisky, A. B.; Clementi, C. Dynamics of Polymer Translocation through Nanopores: Theory Meets Experiment. *Phys. Rev. Lett.* **2006**, *96*, 118103.
34. Slonner, G. M.; van den Hout, M.; Broekmans, O.; Dekker, C.; Dekker, N. H. Distinguishing Single- and Double-Stranded Nucleic Acid Molecules Using Solid-State Nanopores. *Nano Lett.* **2009**, *9*, 2953–2960.
35. Kowalcyzk, S. W.; Grosberg, A. Y.; Rabin, Y.; Dekker, C. Modeling the Conductance and DNA Blockade of Solid-State Nanopores. *Nanotechnology* **2011**, *22*, 315101.